Optimizing diffusion time prior to probe-mediated microwave heating of injected nanoparticles for hyperthermia treatment of tumors

BEE 4530 Computer Aided-Engineering: Applications to Biomedical Processes
Spring 2013
Biological and Environmental Engineering, Cornell University, Ithaca, NY

Group 9: Colin Enderlein, Rohiverth Guarecuco, Rafael Lizarralde, Erik Rasmussen

Table of Contents

I. Executive Summary

Localized tumor hyperthermia therapy is a treatment that involves heating cancerous tissue to temperatures that result in tumor cell necrosis, while preventing damage to surrounding healthy tissue. Hyperthermia therapy treatments reported in the literature have shown that nanoparticles can be injected into a targeted tumor, allowing specific regions to undergo treatment and reducing the healthy tissue that is affected as well. Previous studies have shown that when the nanoparticles absorb specific wavelengths of radiation, they undergo resonance and emit heat. Thus, the targeted tumor can be heated through the actions of both tissue absorption, and heat emitted by the excited nanoparticles. This additional heat due to nanoparticles within a tumor can facilitate tumor heating over a given time-frame so as to prevent damage to surrounding healthy tissue. Our project aimed to investigate the efficacy of utilizing injectable ferromagnetic nanoparticles (with the properties of γ-hematite nanoparticles) to facilitate microwave heating of cancerous tissue.

The first stage of our project was modeling the precise delivery and dispersion of a volume of nanoparticles in a targeted cancerous tissue. To do this, we built a 1D radially symmetric computational model in COMSOL to represent a tumor, and we computed the diffusion profile of the nanoparticles in this domain over the time directly after injection. Next, we built a 2D axisymmetric computational domain in COMSOL to model the heat treatment. This model included heating of the tumor tissue with a microwave probe, and then coupled this heating with heating due to the nanoparticle concentration in the tissue. Computing the heat and energy profiles for this heating model allowed us to then determine the optimal time after injection to begin the heat treatment to maximize cancer cell death, but minimize damage to healthy tissue. The optimal time was determined as the time when all cancerous tissue temperature had been raised above 43 °C, while the maximum surrounding healthy tissue temperature was still below 43 °C. In conjunction with finding the optimal heating interval, our goal was to also find the optimized injection nanoparticle concentration, nanoparticle diffusion time, and microwave radiation power level.

Computed temperature profiles that took into account heating due to the presence of nanoparticles within the tumor computational domain showed only a slightly larger proportion of the tumor domain reaching temperatures in excess of 43 °C than could be achieved when heating is due to radiation absorption by the tissue alone. Our conclusion is that, within the model, the nanoparticles are indeed absorbing microwave radiation, but they are not subsequently emitting as much heat as was expected. As they are absorbing radiation, they are blocking the passage of energy into the tissue areas directly surrounding the nanoparticles. Without the nanoparticles in the tumor domain, the microwave radiation can be absorbed entirely by the tissue, resulting in more desirable temperature profiles. Thus, our model as implemented does not demonstrate that injecting γ-hematite nanoparticles into a tumor facilitates probe-mediated microwave heating of said tumor. However, several changes could be made to our model to achieve more desirable results. For example, if the nanoparticles were injected so as to enclose the tumor targeted for destruction, then they would effectively create a barrier for microwave radiation to pass through, thus restricting the radiation heating primarily to the enclosed tumor region. Alternatively, the ferromagnetic nanoparticles could be magnetically tuned (using a varying magnetic field) during microwave radiation so that they do actually undergo resonance significantly, resulting in greater

heat emission and desirable temperature profiles. Regardless, we did successfully model probe-mediated microwave radiation of a tumor for hyperthermia treatment using a complete electromagnetism module in COMSOL, something that has never been done before in this course. We found the optimum microwave probe power level and radiation time required to maximize tumor death while minimizing healthy tissue damage in our model. It follows that localized tumor hyperthermia therapy that uses a microwave-emitting probe for tumor destruction can be modeled and fine-tuned using COMSOL. With appropriate model modifications, it could be shown that ferromagnetic nanoparticles can be used to direct the microwave heating in the targeted region. Mass transfer and heat transfer models similar to the ones used in this project can be built with specific tumor geometries, tissue properties, and probe properties, and such models can be used to plan clinical applications of using probe-mediated microwave heating of cancerous tissue.

II. Introduction

Cancer is a generic term that refers to a broad collection of diseases characterized by uncontrolled and unregulated growth of mutated cells. There are over 200 different known cancers that afflict humans [14]. Unlike many diseases, cancer afflicts all demographics, regardless of economic status or other socially derived factors. Taking into account all the forms of this disease, cancer was the cause of 13% of all deaths worldwide in 2008, corresponding to approximately 7.6 million deaths worldwide [14].

Over the last 30 years, cancer treatment has improved markedly. An important measure of the efficacy of cancer treatment is the 5-year relative survival rate. This is the percentage of patients with cancer that are alive five years after their diagnosis divided by the percentage of the general population of corresponding sex and age that are alive after five years. The 5-year relative survival rate in the U.S. has increased from 49% in 1977 to 68% in 2008 [1]. However, despite advances in treatment, the global prevalence of cancer continues to increase largely due to longer average life expectancy and increased risk factors in certain areas, such as limited access to cancer-reducing vaccinations and early-detection examinations [5]. Given current projections, in 2030 it is estimated that 13-17 million people will die from cancer worldwide [14].

The most common treatments of cancer are surgical tumor removal, radiation therapy, and chemotherapy [1]. Although relatively effective, these treatments are far from ideal. Surgical tumor removal is extremely invasive, while chemo and radiation therapies can present serious side effects. Thus, there is an increasing demand for treatments that are effective, but minimize invasiveness and undesirable side effects. Often the treatments that meet these requirements involve mechanisms for specifically targeting cancer cells while rendering healthy tissue unaffected. For example, antibodies specific to cancer cell surfaces can be used to deliver drugs or radiation directly to tumors, and new drugs are continually being developed that are better at distinguishing between malignant and normal cells [9]. One technique for specifically targeting tumors that has gained interest due to its economic feasibility and minimal potential for side effects is thermal therapy.

Thermal therapy applies extreme cold, cryotherapy, or extreme heat, hyperthermia therapy, to the tumor with the objective of killing all the malignant tissue. We will explore thermal therapy in

this study, but we will only examine hyperthermia therapy because it has been shown that cancerous cells are particularly sensitive to high temperature compared to normal cells [12]. Hyperthermia therapy destroys tumors by heating them to temperatures greater than 43 °C. This temperature range has been shown to be effective at killing cancer cells [10]. For use in this study, we will utilize the concept *cumulative equivalent minutes* for T = 43°C, or CEM43°C, which standardizes the amount of hyperthermia treatment in terms of 43°C.

One of the limitations of hyperthermia therapy is that when sufficiently heating tumor tissue for destruction it is inevitable that some surrounding healthy tissue will be destroyed. Thus, the success of hyperthermia therapy hinges on the ability to specifically target the area of interest. Several methods of localizing electromagnetic radiation, and its subsequent heating, to the tumor have been developed in the literature [4,6,10,12]. One method uses a microwave-emitting probe that can be inserted directly into the tumor [6]. Another proven method of localization involves injecting γ-hematite (Fe_2O_3) nanoparticles into the tumor, which can then be excited with microwaves [10]. In this study we will examine the effect of combining these two localization strategies. Although both of these strategies have been proven in isolation, the effect of combining them has not previously been studied.

Specifically, the use of γ-hematite nanoparticles excited with a microwave frequency of 2.45 GHz has been proven to be effective at raising tumor temperatures to the necessary critical levels for treatment [10]. Therefore, in this study we will model the use of a 2.45 GHz emitting probe inserted directly into the tumor in conjunction with injected γ-hematite nanoparticles. The nanoparticles will be assumed to be injected directly into the center of the tumor, after which they diffuse outward radially. Previous research has shown that both the distribution of nanoparticles and the duration of electromagnetic heating have large influences on the success of the treatment [12]. Thus, the goal of this study is to optimize nanoparticle diffusion time and duration of microwave heating. An optimized solution will achieve total tumor destruction, while minimizing healthy tissue damage.

III.Design Objectives

1. Develop a diffusion profile of the nanoparticles over time.
2. Ensure total tumor destruction by reaching a lethal CEM43°C value
3. Minimize damage to healthy tissue by keeping it below its lethal CEM43°C value
4. Determine the optimal time after injection to begin microwave radiation.
5. Determine the optimal duration of microwave radiation heating.

IV. Methods

IV.a. Model Development

Using the guiding design objectives previously stated, we were able to formulate this physical problem into one that can be interpreted by COMSOL. One of the first steps in developing this model was to define the computational domain over which the physics would be applied. This involved not only determining the dimensions of our model, but assessing what boundary conditions are appropriate. Given that our model incorporates physics for mass transfer, heat transfer, and Maxwell's equations for electrodynamics, the computational domains are physically represented differently with their own boundary conditions. These various domains can be seen below.

IV.b. Schematic

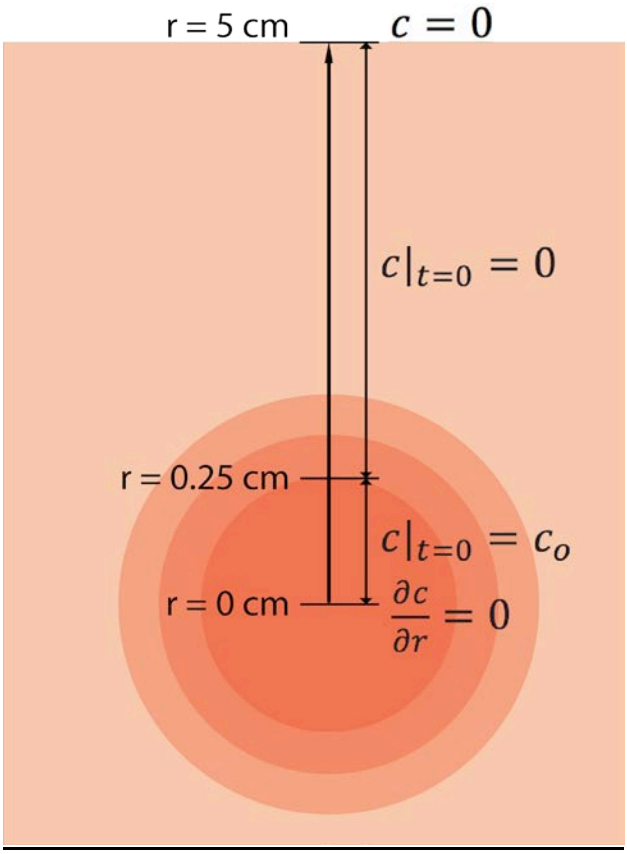

FIGURE 1. Mass transfer (1D radially symmetric): This figure represents the temporal radial movement of nanoparticles after initial injection within the volume represented by r = 0.25cm.

For mass transfer computations, the domain is assumed to be homogenous in terms of material properties, and the boundary condition used is a pseudo infinite approximation whereby

concentration far from the injection site is zero. Diffusion will follow a 1D radial symmetric governing equation given by equation 1.

$$D_{AB}\frac{1}{r}\frac{\partial}{\partial r}\left(r\frac{\partial c_A}{\partial r}\right)=\frac{\partial c_A}{\partial t} \quad \text{.....(1)}$$

D_{AB} is the diffusion coefficient in m^2/s, c_A is concentration in mol/m^3, r is radial position in meters, and t is time in seconds. The purpose of the particles is to help direct the exact heating area from the microwave probe, which involves the use of both heat transfer and Maxwell's equations.

In examining the physics associated with microwave heating, it is useful to visualize a slightly different physical domain as given in Figure 2.

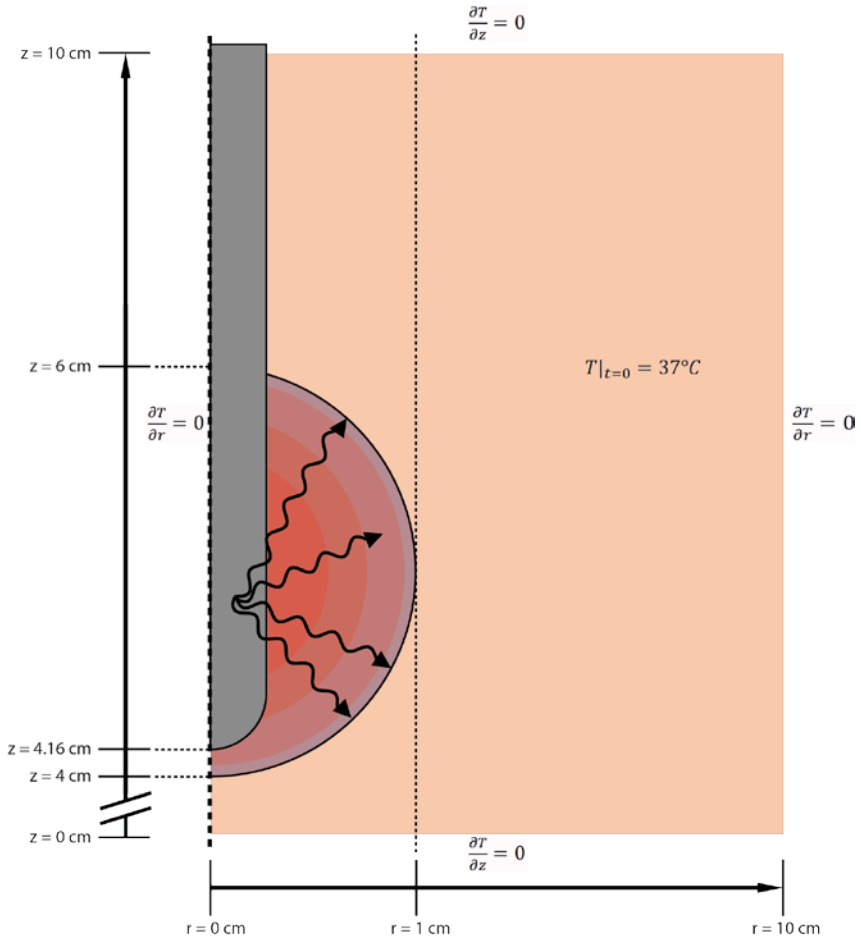

FIGURE 2. Heat transfer (2D axisymmetric): This figure represents the temporal heating front produced from the microwave probe (grey cylinder on left wall), moving outward from r = 0cm to the outer edge of the tumor given by r = 1cm.

Figure 2 yet again incorporates a pseudo infinite assumption; the temperature fluxes at locations distant from the probe are assumed to be zero. The heating will be modeled with a 2D axisymmetric equation as given by equation 2.

$$\rho C_p \frac{\partial T}{\partial t} = k\left[\frac{1}{r}\frac{\partial}{\partial r}\left(r\frac{\partial T}{\partial r}\right) + \frac{\partial}{\partial z}\left(\frac{\partial T}{\partial z}\right)\right] + Q_{□□□} + Q_{□□□} \quad (2)$$

Here ρ is liver density (kg/m^3), C_p is specific heat (J/(kg*K)), k is thermal conductivity (W/(m*k)), r is radial position in meters, z is vertical position in meters, t is time in seconds, Q_{bio} is the blood perfusion heat source term, and Q_{mic} is the is the microwave heating heat source term, which is the component that couples equation 2 to the electrical heating modeled by Maxwell's equations. The microwave heating in the tissue is modeled by equation 3.

$$\nabla \times \mu_r^{-1}(\nabla \times E) - k_0^2\left(\varepsilon_r - \frac{j\sigma}{\omega\varepsilon_0}\right)E = 0 \quad (3)$$

Here $\mu_{□}$ is the relative permeability (unitless), E is the electric field (V/m), $□_0$ is the wave number of free space (rad/m), ε_r is the relative permittivity (unitless), j is a scalar multiplier in the formula for the complex eigenfrequency (rad/s^2), σ is the electric conductivity (S/m), ω is the angular frequency (rad/s), and ε_0 is the permittivity of free space (F/m). Additionally, the boundary conditions for the probe are designated as input power at the top of the dielectric, and then a scattering boundary condition is used on the on the three walls not containing the probe. A scattering boundary condition is where waves orthogonal to the wall escape the surrounding tissue, while waves at other angles are reflected back into the tissue.

The specific geometry for this probe can be seen in Figure 3.

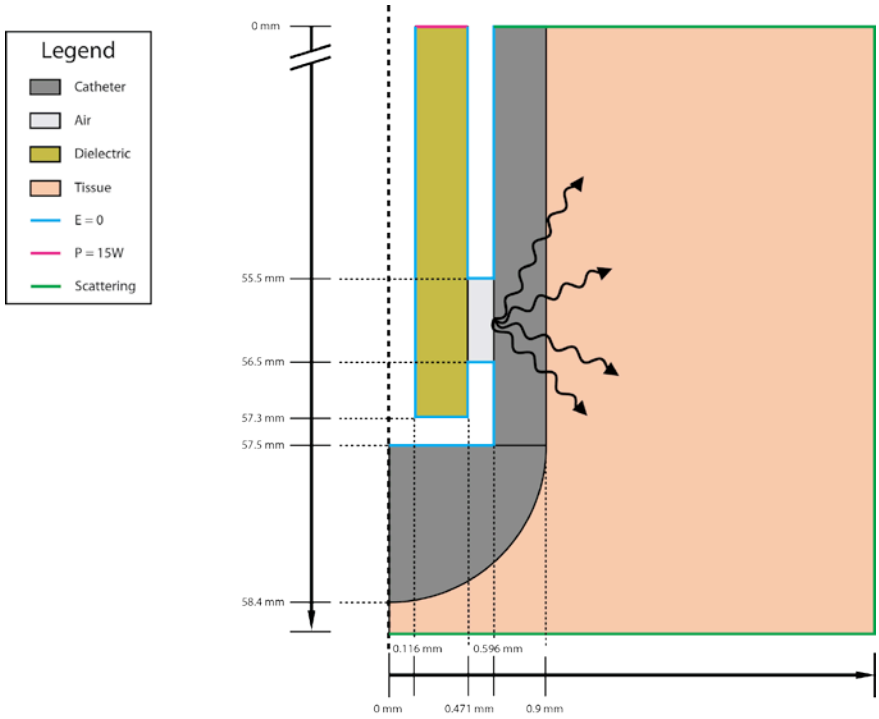

FIGURE 3. Probe schematic showing energy release through the air window between dielectric and catheter wall.

While the material properties of liver tissue in the domain given by Figure 2 are assumed to be constant, the inclusion of nanoparticles is assumed to change the electrical properties depending on the local concentration. This was incorporated into our model by finding values for nanoparticle electrical properties in the literature on a per 25% volume fraction basis, and then extrapolating how lower fractions would influence the tissue. This is presented in more detail when discussing the parameters in Table 1, as seen in Appendix A.

The values presented in Table 1 were accumulated through investigating existing literature on models that show similarity to ours. As previously mentioned, while some parameters (such as those associated with mass and heat transfer) remain constant, it is assumed that the electrical properties are altered by the presence of nanoparticles. Because particle permittivity and permeability are given on a volume fraction basis, this allows the incorporation of these parameters into those of the liver. Equation 4 represents how the permittivity in the liver can be adjusted to include the presence of particles.

eps_liver*(1−v_c)+(v_c/0.25)*(eps_p25+i*eps_dp25).....(4)

Here, eps_liver, eps_p25, and eps_dp25 are defined in Table 1, i represents the imaginary portion of the relative permittivity, and v_c is the volume fraction as a function of particle concentration, given by particle concentration multiplied by particle volume and Avogadro's number. This method seen in equation 4 can similarly be employed to compute for the corrected permeability and conductivity values.

With the previously mentioned parameters, the physics functions included in COMSOL are able to implement our governing equations and boundary conditions without much more numeric manipulation. The process of coupling the different physics starts by running the diffusion module, the final concentration profile of which is passed to the EM heating module for use in modifying the local electrical properties through the use of equation 4 and its counterparts for electrical permeability and conductivity. The next phase is to run the EM heating physics, where the microwave power input, P_in is applied for t_heat amount of time, and then the heat is allowed to dissipate over the period of t_cool. This microwave heating effectively acts as a source term for the bio-heat physics module, which translates the energy density profile created by the microwave input into heat generation within the tissue.

V. Results and Discussion

V.a. Optimization Goals

One of the most critical components of developing a computational model is to optimize the parameters so as to predict the best conceivable results. In the case of our model, the initial goal was to optimize c_max, t_diff, P_in, and t_heat so as to maximize tumor ablation and minimize healthy tissue ablation. However, as will be discussed later, it has become apparent from our model that particles are not undergoing heat generation when exposed to the microwave field, and therefore heating results after diffusion has occurred vary minutely from the model when no particles are present. Therefore, the primary parameters we will be interested in optimizing are P_in and t_heat.

The success of model optimization is judged through the use of an objective function. In our case, we are using *cumulative equivalent minutes* for T = 43°C, or CEM43°C. What this provides is a normalizing equation for our model that presents heating time at different temperatures in terms of the equivalent time that would be observed at 43°C for the same damage to occur. For example, a minute at 50°C is equivalent to 128 minutes at 43°C, so over this minute, the tissue experiences 128 minutes of CEM43°C. Equation 5 shows the CEM43°C function.

$$\text{CEM43°} = \square\square * \square^{43-\square} \quad \text{.....(5)}$$

In equation 5, Δt is the time interval in minutes, and R is a constant equal to 0.5 when temperatures exceed 43°C or equal to 0.25 when temperatures are below 43°C [3]. T is the average temperature of the region of interest during the time interval t, and if T is not constant over time, CEM43°C must be integrated over the time interval of interest.

When implementing this equation as part of our objective function, the goal will be to have the CEM43°C values for the tumor domain reach lethal levels while minimizing necrosis to healthy tissue, which will be quantified by the volume of tumor tissue that reaches lethal CEM43°C values minus the volume of healthy tissue that reaches lethal CEM43°C temperatures. Implementation of this function will be discussed in more detail later.

V.b. Preliminary Results

Following the model outlined in the previous section, surface plots of radiation energy density and temperature were developed. Additionally, diffusion of the nanoparticles is modeled assuming the injection volume is 0.065 cm^3, and then the profile is plotted after diffusion has progressed over 10 hours.

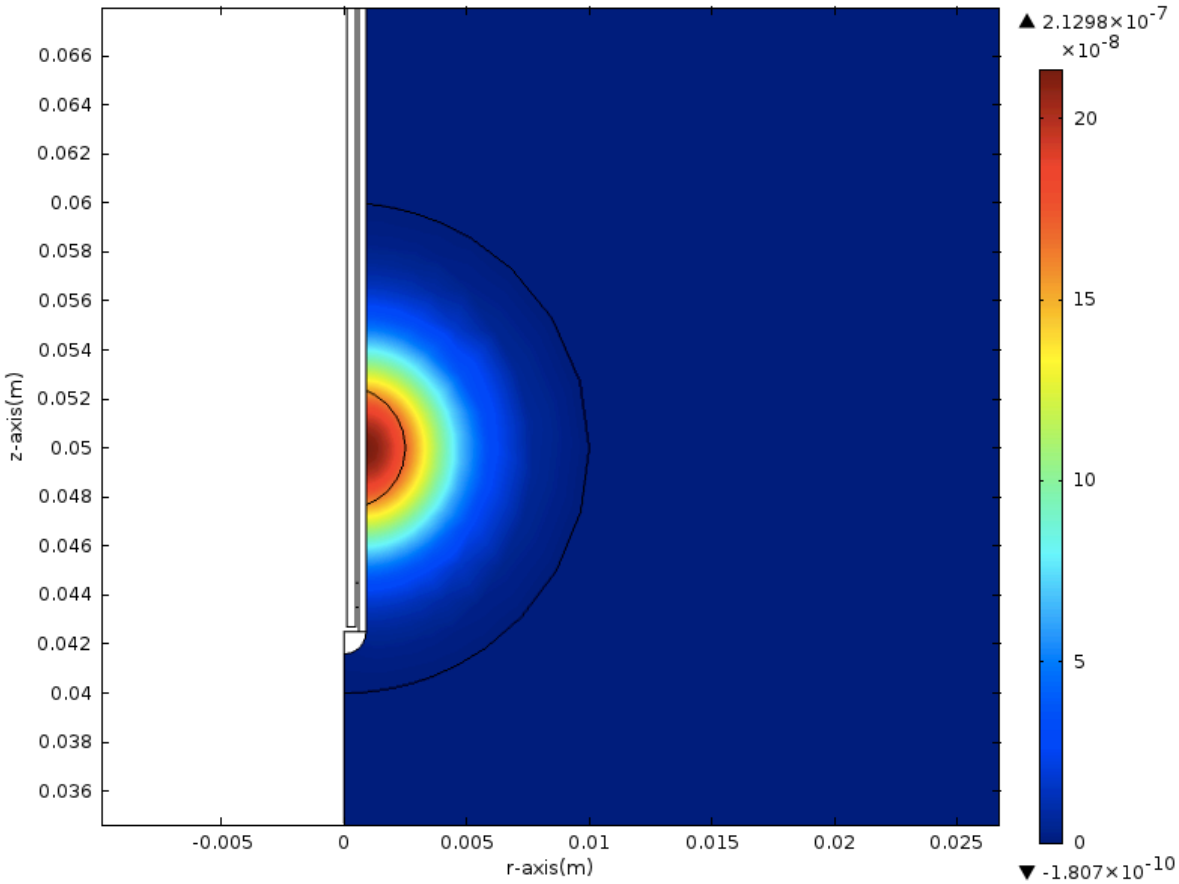

FIGURE 4. Model diffusion profile after 10 hours have elapsed from initial injection. Concentration is in mol/m^3.

The surface plot presented in figure 4 is indicative of our initial iteration of calculating a diffusion profile. As mentioned previously, this profile ultimately has little effect on the electric and heating profiles generated by our model.

While including the nanoparticle concentration in this model is one of the pivotal aspects behind this novel cancer treatment, it is important to assess precisely how the presence of these particles influences both energy dissipation in the tissue, and the overall heating profiles developed over time.

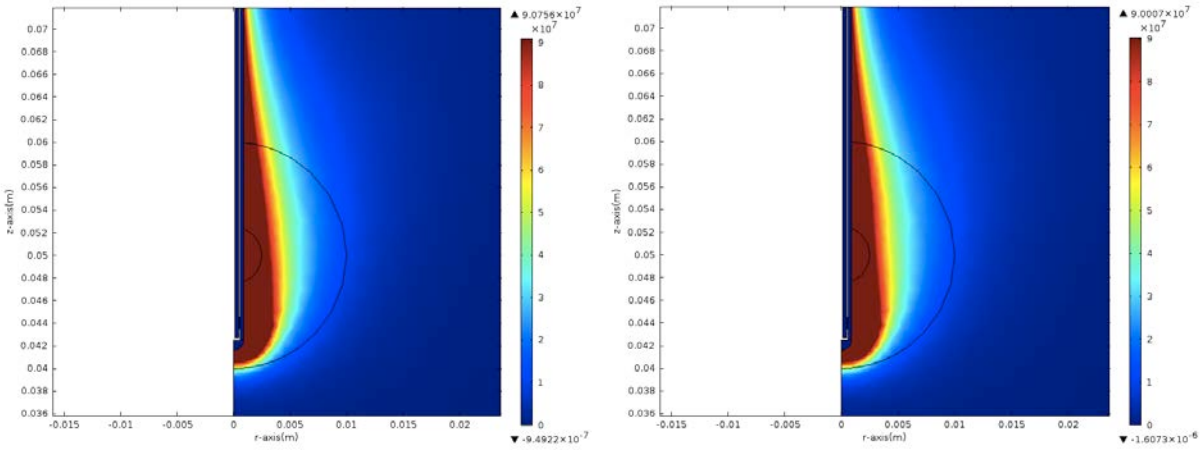

a. **b.**

FIGURE 5. a. Energy dissipation profile (W/m^2) without nanoparticles **b.** Energy profile with nanoparticles considered.

Figure 5 shows the energy dissipation in W/m^2 generated from the probe during situations when there is tissue heating alone, and when the electrical characteristics of the tissue are coupled with those of the nanoparticles at varying concentrations. Consistent with this minute change in electric field, the temperature surface plots similarly demonstrate that nanoparticles do not significantly increase the heat generation over the domain.

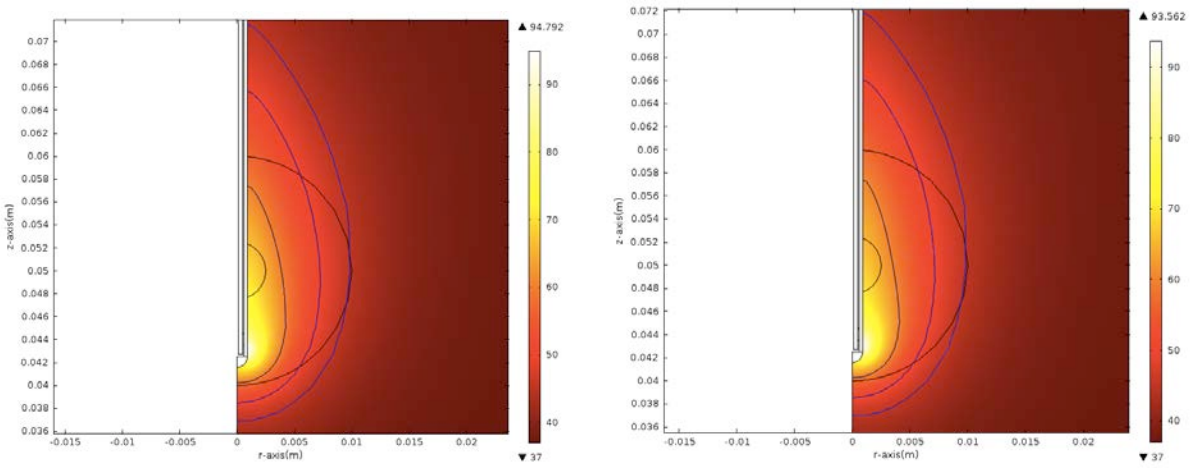

a. **b.**

FIGURE 6. **a.** Temperature profile (°C) without nanparticles considered **b.** temperature profile with nanoparticles considered

Figure 6 shows the temperature profiles generated with the conditions of nanoparticles not present (a.) and when they are present (b.) The background surface plot represents the profile for all temperatures recorded, and the three contour lines designate 45, 50, and 60°C from right to left. Note that the maximum attained temperatures shift by barely 1.2°C between the plots with and without particles, and the contour lines barely shift, which further validates that the presence of diffuse nanoparticles has only a minimal effect on the end heating profile. However, the particles can still in fact guide heating by absorbing microwave energy, which will be explained in more detail shortly.

The results observed in figures 5 and 6 can be further elucidated by observing temperature profiles developed shortly after injection.

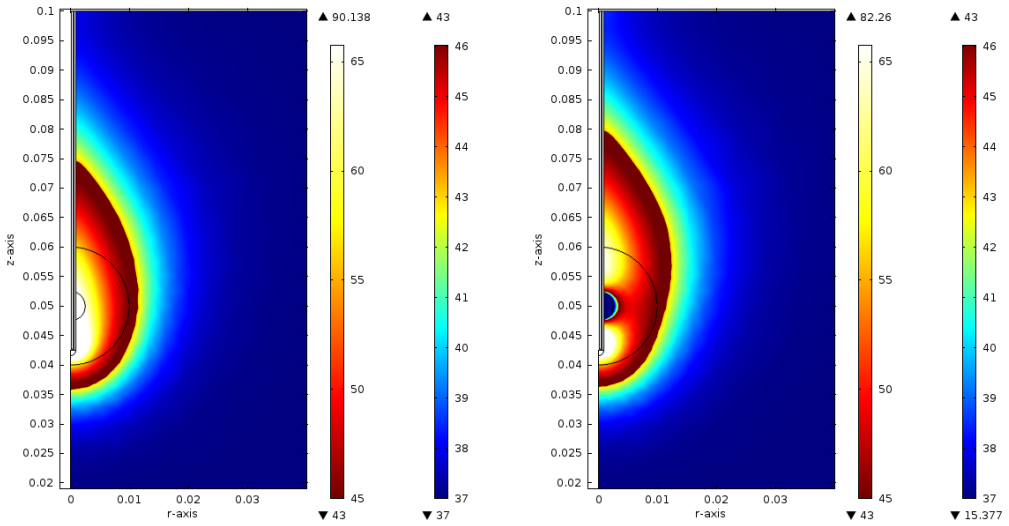

a. **b.**

FIGURE 7: a. This shows a temperature profile plot (°C) when no nanoparticles are present in the model. The rainbow color scheme designates temperatures from 37 to 43°C, while the red/yellow scheme indicates areas of higher temperature. **b.** This surface plot includes the presence of particles in the initial injection site after no diffusion has been allowed to progress.

From Figure 7, it is evident that rather than the nanoparticles acting as a heat source upon exposure to microwave radiation, they are in fact effectively blocking the passage of energy into this tissue area. Around the nanoparticle site, temperatures are much lower than when no particles are present, indicating that the particles are actually absorbing the microwave radiation and not emitting nearly as much heat as is released from tissue energy absorption. While this is not the result we anticipated, this energy absorption behavior could still be utilized in conjunction with microwave probe heating and varied injection sites in order to act as a barrier through which energy cannot pass, effectively creating a specified region for heating to occur. The reason why these effects are not observed after diffusion has been allowed to progress for many hours is that the particle density is sparse enough that tissue electric properties are predominantly considered, resulting in energy and heating profiles that appear the same as though no particles had been injected at all.

V.c. Optimized Results

In order to implement the CEM43°C as our objective function, it is necessary to find values that are representative of lethal CEM43°C exposure times. Values such as these are obtained experimentally, and from a literature search are taken to be CEM43°C = 340 min for healthy liver tissue [3], and CEM43°C = 10 min for tumor tissue [2]. These values are represented by t43c_tiss and t43c_tum for liver and tumor tissue respectively, and are in units of seconds.

For implementation into COMSOL, we utilized the built in diffusion module and defined equation 5 as a reaction source term. The solver would then effectively treat 1 mol/m^3 as equivalent to 1 s CEM43°C, removing the need to implement this function through a differential equation. We created 2 diffusion modules, one for the tumor domain, and one for the healthy tissue, which was found to yield more reliable results than combining the two, due to the lethal CEM43°C thresholds being of different orders of magnitude. To further maintain numerical accuracy, the reaction (at a given location) was halted after lethal CEM43°C was reached, using a Boolean operator, (otherwise, the CEM43° can climb extraordinarily high and reduce accuracy along the boundaries of tissue that only just reach the threshold). R is also found by using a Boolean operator dependent on the current temperature, as given by equation 6, below.

R = (T>=(43[degC]))*0.5+(T<(43[degC]))*0.25 .....(6)

CEM43°C was normalized over each region (tumor and healthy tissue) using the following functions, so as to incorporate partial damage while ignoring damage beyond the lethality threshold:

t43n_tumor = min(t43_tum,t43c_tum)/t43c_tum .....(7)
t43n_tissue = min(t43_tiss,t43c_tiss)/t43c_tiss .....(8)

This brings the CEM43°C evaluation for each region to within the range of zero to one for a unit volume. These functions were then integrated over the volume of the tumor and volume of the healthy tissue to obtain obj_tum and obj_tiss, the two components of the objective function:

obj = obj_tum – obj_tiss .....(9)

This objective can be conceptualized as the difference in the volume-weighted damage to the tumor and the tissue—thus if equal volumes of tissue and tumor die, the objective is zero. To increase readability, the objective function was normalized once again to the best possible outcome: all of the tumor dead, and no damage to healthy tissue. In Table 2 (below), we see the objective in each case as a percentage of the objective of this perfect outcome.

Table 2. Optimized results from the parametric sweep against heating time and input power. The green regions represent the highest rates of success for the objective function with the highest equating to a 95.5% success from P_in = 10W and t_heat = 420s.

		P_in [W]									
		5	10	15	20	25	30	35	40	45	50
t_heat [s]	60				48.2%	64.8%	78.2%	86.3%			
	120		35.5%		92.1%	85.7%	71.9%		31.3%		-24.3%
	180			94.2%	83.5%	62.0%					
	240		72.9%	90.7%	69.3%		-17.4%		-134.4%		-229.8%
	300		87.6%	84.5%							
	360	28.0%	94.1%	78.0%	36.1%		-108.8%		-238.4%		-366.7%
	420	33.1%	95.5%								
	480	37.4%	94.0%		3.6%		-169.6%		-316.8%		-460.8%
	540	41.0%									
	600	44.5%	91.0%		-25.2%		-209.7%		-380.5%		-530.7%

From the results in Table 2, it is apparent that there are a range of values that enable high success rates from our objective function. Notably, the most successful results are obtained with a power input of 10 W for 420 s of heating. In this case, all of the tumor dies, so the 4.5% error is caused by healthy tissue damage. These results are strictly from probe heating with no contribution from the particles, but the previously displayed results indicate that high concentrations of particles can may be useful for effectively containing the energy profile, thus reducing ambient heating.

Using the results from Table 2, the objective function can be plotted as seen below in Figure 8, below.

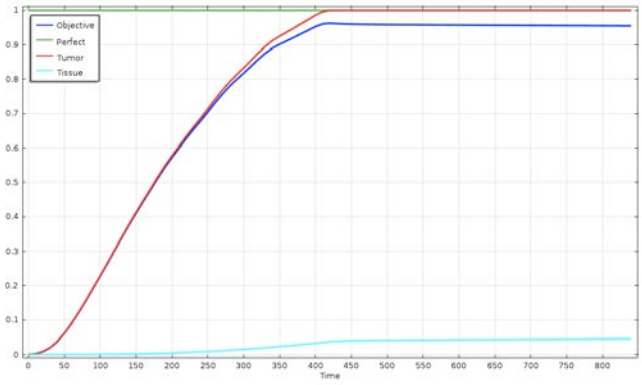

FIGURE 8. This shows the objective function obtained from utilizing the optimized results of P_in = 10W and t_heat = 420s, and the data is presented as a percentage of tumor and healthy tissue that reaches their critical temperature over time. The green line at the top represents the ideal situation where all tumor tissue dies and no healthy tissue is harmed, and the objective line in blue is the difference between the tumor and tissue curves.

From Figure 8, given that the results for a 95.5% success rate are utilized, it makes sense that the true objective function, as seen in blue, plateaus out very close to the optimum possible results. As seen in Table 2, there are a number of power inputs and heating time combinations that can provide high success rates given our objective function, and while certain characteristics of the objective plot may change with these altered parameters, the main characteristic of success is plateauing of the objective function close to the perfect condition line.

V.d. Accuracy Check

In order to help verify the validity of our model, our computed results can be compared against existing experimental research.

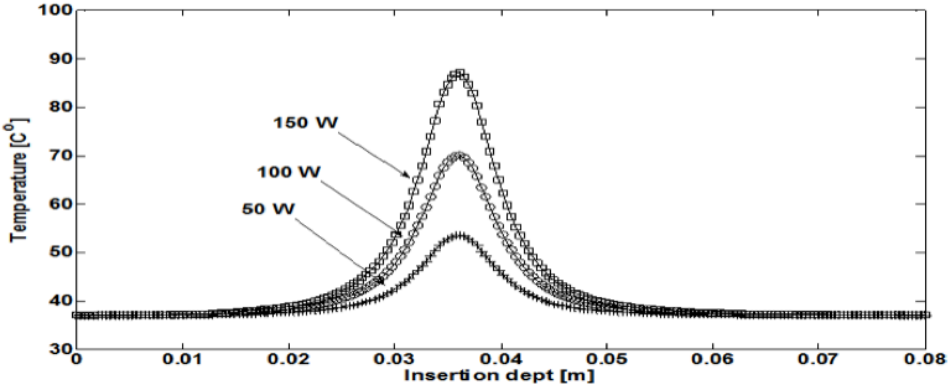

FIGURE 9. Probe experimental heating effects: (Wongtrairat, 2011)[13] These curves represent temperatures in porcine liver tissue with depth along the side of a microwave heating probe that is activated for 60s at either 50, 100, or 150W. The observation line runs 5mm away and parallel to the microwave probe. Microwave frequency is also 2.45 GHz here.

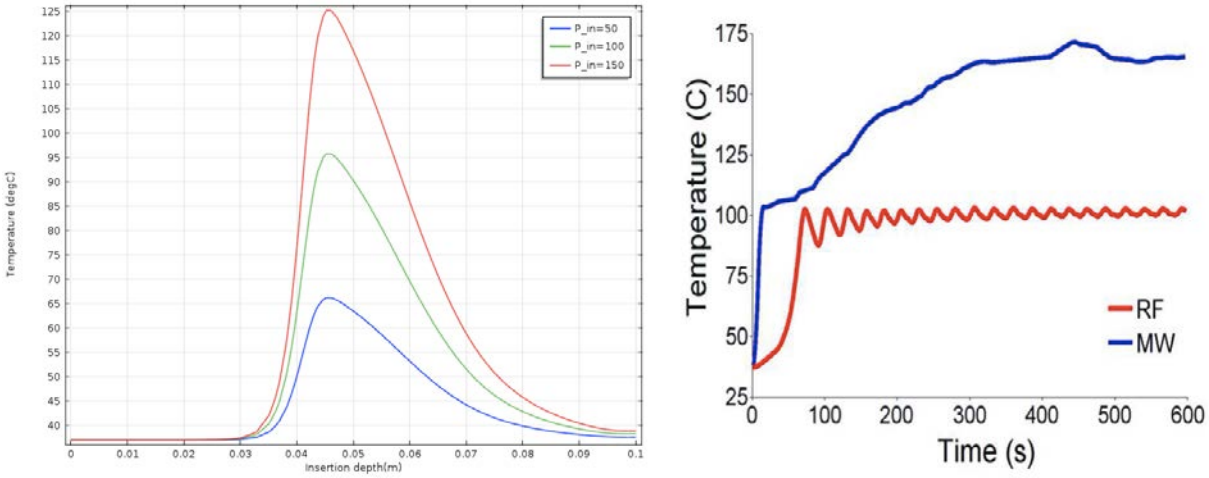

a. **b.**

FIGURE 10. Probe accuracy check: a. Computed plot of cut line 5 mm from probe after 60s of heating at varying power inputs. **b.** (Lubner, 2010)[4] the blue line is a plot of microwave heating of porcine tissue with a power input of 50W.

From our computed accuracy check seen in figure 10 a to verify that strictly probe-heating results are consistent with findings in the literature, we can see that the maximum computed temperature values from our model exceed the results seen in Figure 9 by up to 38%. However, the general trend observed between lines of varying energy input are consistent between experimental and computed results, indicating that our model reacts to changes in input energy in a way that is consistent with the experimental results. From comparing our analytical results to the experimentally collected ones, the higher temperatures observed in our model could

potentially be accounted for by the exclusion of parameters to take water vaporization into account. The drop off in slope of Figure 10 b at 100°C results from boiling point being reached, In our actual model, we do not reach temperatures exceeding 100°C, so have not included parameters to account for the latent heat of vaporization, which would diminish the temperature of our model values though energy absorption to drive phase change.

Another important accuracy check to consider is the specific heating effects of the excited nanoparticles.

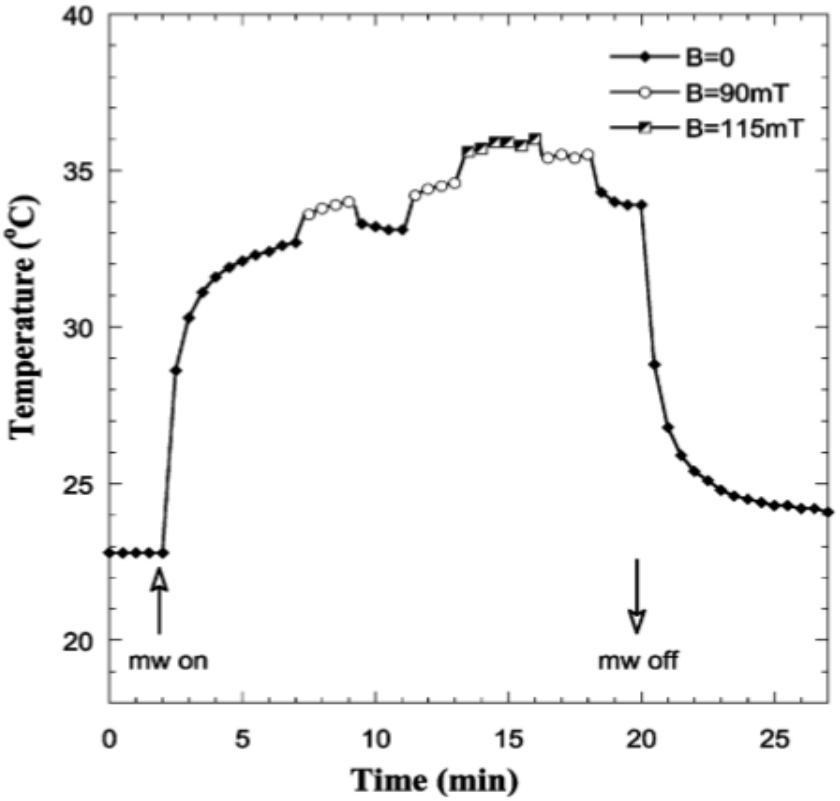

FIGURE 11. Particle experimental heating effects (Sakran, 2004)[5] These data show the change in surface temperature of 30-250 nm diameter magnetite nanoparticles heated with microwave frequencies of 9.2 GHz and power input of 0.5 W. The legend on the upper right designates changes in magnetic field that yield small variances in particle surface temperature. The rapid initial increase in temperature is due to microwave heating of the ambient acrylic, while the subsequent magnetic tuning results in variations of 2-3°C caused by particle resonance.

To compare to our model, we will utilize these same parameters for probe heating with nanoparticles being considered.

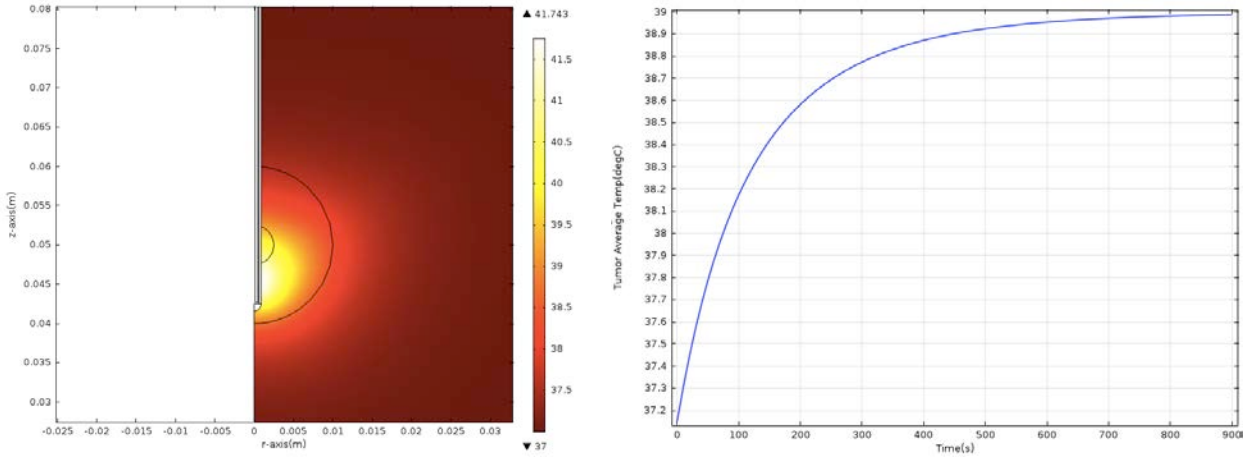

a. **b.**

F**IGURE 12. a. Particle accuracy check**: Heating conducted with power = 0.5 W and frequency = 9.2 GHz for 900 s. **b.** Accuracy check average temperature over tumor domain.

Figure 12 shows the heat profile attained after 900 s of heating with particles considered, power input = 0.5 W, and frequency = 9.2 GHz. While the maximum change in temperature seen in Figure 12 a is only about 4.7°C as compared to the approximately 12°C change seen in the experimental results in Figure 11, an important note to consider is that the experimental results only consider the change in temperature of the particles and surrounding acrylic, whereas our model incorporates thermal properties of the liver tissue on a much larger domain. Therefore, it is reasonable to observe that there is less temperature change in our model, which could potentially be accounted for by replacing tissue electrical and thermal properties with those of the acrylic. Additionally, as previously discussed, given that our model indicates that nanoparticles are absorbing energy but not necessarily emitting much heat, it is reasonable to assume that the behavior observed in Figure 12 is strictly from microwave heating of the tissue.

As a continuation to the experimental results seen in Figure 11, Sakran proposed that the increase in temperature of magnetite nanoparticles embedded in acrylic could be modeled by equation 7.

$$\Delta\square = \frac{\square}{4\square\square\square} \quad \text{.....(10)}$$

Where P is the power absorbed by the particles, k is the thermal conductivity of the surrounding media, and r is the radius of the nanoparticles. As compared to the results of Sakran where a 2-3°C change was expected from nanoparticle heating, it would be beneficial to include a varying magnetic field in our model to see if the steady state temperature of Figure 12 b is perturbed.

V.e. Sensitivity Analysis

In order to ascertain how sensitive our model is to changes in some of our assigned parameters, we conduct a sensitivity analysis that computes the solutions over a range of defined parameters.

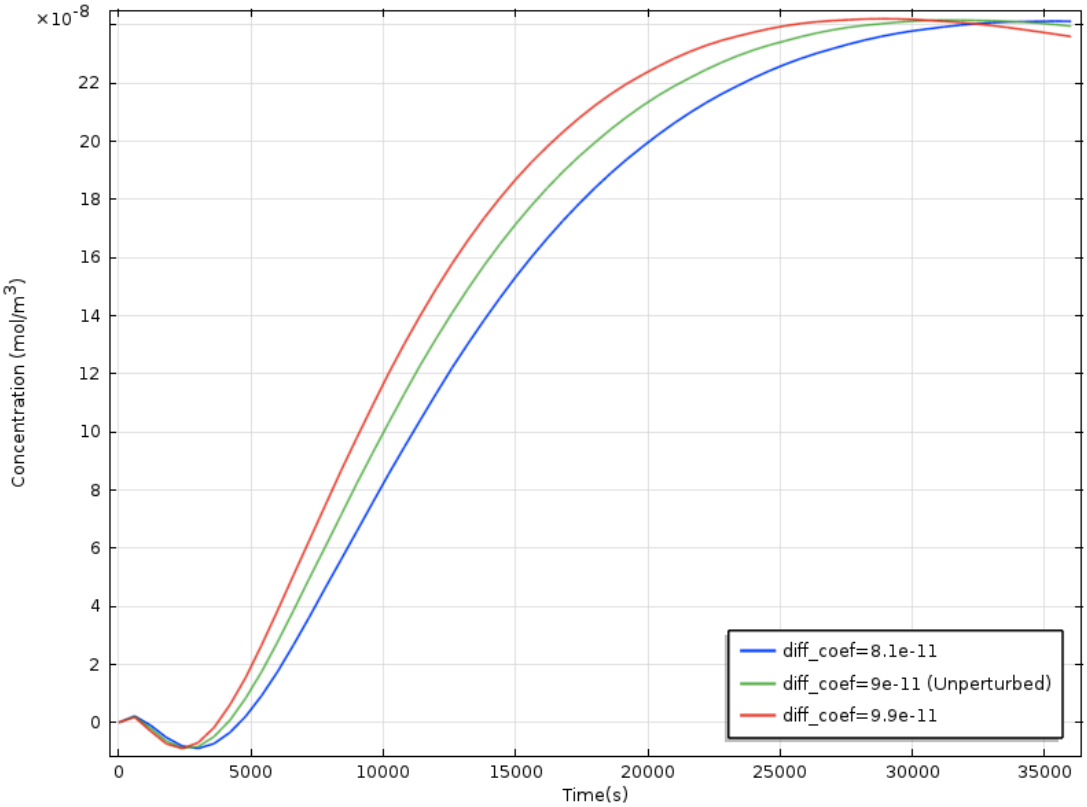

FIGURE 13. Varying diffusion coefficient (diff_coef) sensitivity analysis.

Figure 13 shows the changes in concentration values with time at a point 0.005 m from the center of the tumor while changing the particle diffusion coefficient with a constant initial concentration of $1.661*10^{-6}$ mol/m^3. The values inputted for diffusion coefficient are +/- 10 % of our model value of $9*10^{-11}$ m^2/s. From this figure, we can see that while the curves are dependent to some extent on diffusion coefficient, the final concentration values after 10 hours of diffusion vary by less than 1.67% from the unperturbed value. This indicates that our model is not highly sensitive to diffusion coefficient values. In order to develop further certainty in these values, physical experimentation would need to be conducted for the particular sized particles of interest within both liver and tumor tissue.

For thermal and electromagnetic properties, we used coefficients for our input parameters (for a parameter denoted “eps_dp25”, the coefficient was labeled “eps_dp25_coeff”). Variations were introduced by performing a parametric sweep over coefficient values of 0.9 and 1.1 (10% changes), with a comparison to coefficients of 1 (the unperturbed parameters).

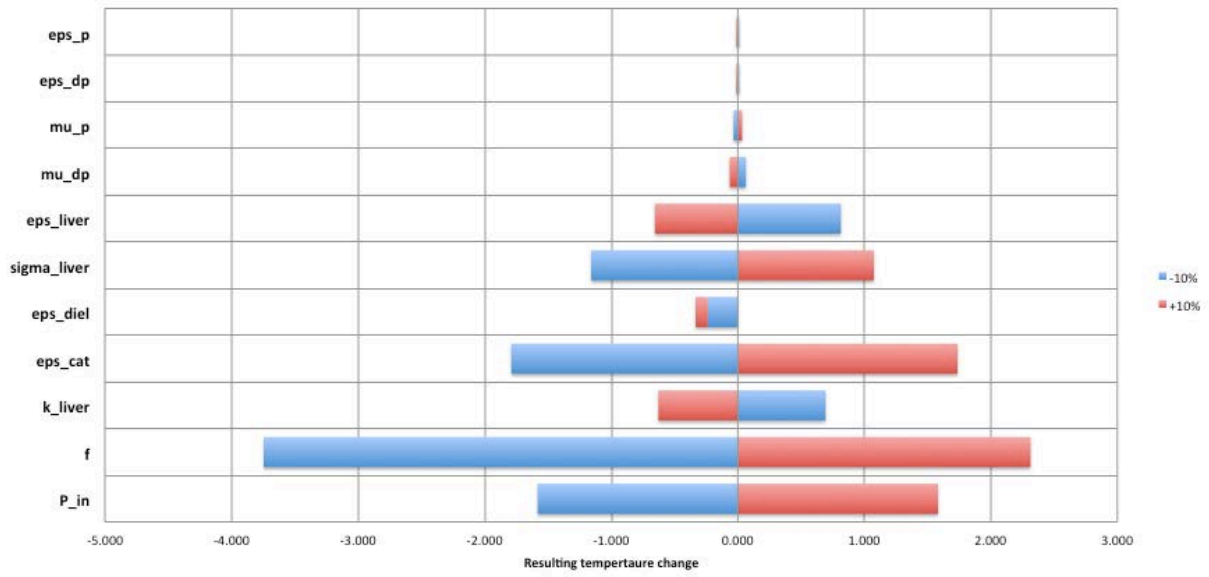

FIGURE 14. Thermal and electrical property sensitivity analysis: The red bars are indicative of a +10% modification to our model parameter (shown on left axis), and the blue bars represent a -10% change. The length of the bars indicates variation from the model computed temperature of 52.82°C.

From Figure 14, it is apparent that most of these parameters do not heavily influence the results obtained in our model. The largest change presented by the frequency parameter, f, resulted in a -3.7°C change in model temperature, which is significant given that this equates to approximately a 7% change from the model. However, our model frequency of 2.45 GHz is a commonly recognized ISM band for use in microwave heating. The next largest variation is caused by the relative permittivity of the catheter (eps_cat), which is a measure of the material's ability to store electromagnetic radiation. Given that our model value for eps_cat was taken from previous experimental work with a similar microwave probe, this value is taken as considerably reliable. Finally, changes in power input (P_in) does illicit a notable temperature change in the model, but given that this is a parameter that will be used for system optimization, it is reassuring to see that changing it does result in alterations of the final results. The remaining parameters illicit no more than a 2% change in computed temperature values, indicating that the system is not heavily sensitive to their change.

VI. Conclusion and Design Recommendations

We varied the nanoparticle injection concentration, and time after injection to determine what combination of these parameters gave a nanoparticle concentration in the tumor that allowed us to use a realistic microwave power for achieving tumor destruction while damaging as little healthy tissue as possible. An objective function was used to determine the optimal duration of microwave radiation heating. We assumed the tumor region needed to be above 43 °C for destruction, and that the healthy tissue needed to stay below 43°C to prevent destruction. Our objective function reflected this and was computed as a function of heating time to determine the optimal heating time.

Through the development of this computational model, it is apparent that our overall system has the potential for use in targeted tumor heating that minimizes the damage to surrounding healthy tissue. For the specific situation modeled, the optimal parameters were found to be an input power of 10W over a period of 420s, allowing for a 95.5% success rate of killing tumor tissue while preserving healthy liver. While these are optimized for one particular situation, the inclusion of different tumor geometries and thermal and electric parameters can easily be modified so as to optimize the treatment of different situations.

Based on our computed results where the nanoparticles do not emit heat as we expected but effectively diminish the electric field, for future expansion of this model, it would be beneficial to experiment with varying the injection site so as to create a boundary in which heating would be contained. This would still allow probe mediated hyperthermia treatment to be utilized, but to a more controlled extent by protecting the surrounding tissue. Additionally, a continuation of our current model could be developed by including different magnetic field densities around the heating site. As seen from figure 11, this allows a certain degree of tuning to take place so that the particles begin to emit heat when subjected to a microwave field.

Another possible modification to our model could be to experiment with different radiation frequencies. Our model value of 2.45 GHz is a common ISM band frequency, but experimentation with other microwave frequencies could potentially yield improved results. Additionally, it would be good to investigate the use of radiofrequency radiation coupled with nanoparticle hysteresis heating. Radiofrequencies are able to penetrate many centimeters into the tissue, possible removing the need to utilize a probe. While the probe is minimally invasive given its small diameter, it still provides a possible infection site and necessitates more technical training in applying the therapy.

VII. Appendix A: Mathematical Statement of the Problem

The governing equations and boundary conditions are succinctly condensed below.

Governing equations:

Mass Transfer:

$$D_{AB}\frac{1}{r}\frac{\partial}{\partial r}\left(r\frac{\partial c_A}{\partial r}\right)=\frac{\partial c_A}{\partial t}$$

Bio-heat Transfer:

$$\rho C_p\frac{\partial T}{\partial t}=k\left[\frac{1}{r}\frac{\partial}{\partial r}\left(r\frac{\partial T}{\partial r}\right)+\frac{\partial}{\partial z}\left(\frac{\partial T}{\partial z}\right)\right]+Q_{□□□}+Q_{□□□}$$

Microwave heating: Maxwell's equations are used here in a 2D axisymmetric domain.

$$\nabla\times\mu_r^{-1}(\nabla\times E)-k_0^2\left(\varepsilon_r-\frac{j\sigma}{\omega\varepsilon_0}\right)E=0$$

Boundary and Initial conditions:

Mass Transfer:

Boundary conditions:

$\frac{\partial c}{\partial r}|_{r=0}=0$, and $c|_{r=r_{max}}=0$, where r_{max} is sufficient for pseudoinfinite conditions.

Initial conditions:

$c|_{t=0;\, r\le r_{injection}}=c_o$, $c|_{t=0;\, r>r_{injection}}=0$

Heat Transfer:

Boundary conditions:

$\frac{\partial T}{\partial r}|_{r=0}=0$ and $\frac{\partial T}{\partial r}|_{r=r_{max}}=0$, where r_{max} is sufficient for pseudoinfinite conditions.

$\frac{\partial T}{\partial z}|_{z=0}=\frac{\partial T}{\partial z}|_{z=z_{max}}=0$, where z_{max} is sufficient for pseudoinfinite conditions.

Initial conditions:

$T|_{t=0}=37°C$, where $t=0$ is the start of radiation, after the diffusion period.

Microwave energy input:

A power input, P, is defined at the top boundary of the dielectric of the probe, and scattering boundary conditions are applied to the three walls that do not contain the probe.

Table 1. Parameters and Constants used in the development of the model.

Parameters/Constants	COMSOL Name	Value	Source
Blood Density	rho_blood	1000.0 kg/m^3	13
Blood Specific Heat	Cp_blood	3639.0 J/(kg·K)	13
Blood Perfusion Rate	omega_blood	0.0036000 1/s	13
Blood Temperature	T_blood	310.15 K	13
Liver Relative Permittivity	eps_liver	43.030	13
Liver Electric Conductivity	sigma_liver	1.6900 S/m	13
Liver Thermal Conductivity	k_liver	0.56000 W/(m·K)	13
Dielectric Relative Permittivity	eps_diel	2.0300	13
Catheter Relative Permittivity	eps_cat	2.6000	13
Microwave Frequency	f	2.4500E9 Hz	10
Input Microwave Power	P_in	20.000 W	13
Nanoparticle in Tumor Diffusion Coefficient	D	9E-11 m^2/s	7
Nanoparticle Volume	V_particle	6.5450E-23 m^3	10
Default maximum element size	e_max	0.0067000	NA
Initial Nanoparticle Concentration in Injection Domain	c0,1	1.661E-6 mol/m^3	10
Initial Nanoparticle Concentration Everywhere Else	c0,2	0 mol/m^3	NA
Initial Temperature Everywhere	T0	310.15 K	NA
Real permittivity of nanoparticles at 25% volume fraction	eps_p25	5.5	10
Imaginary permittivity of nanoparticles at 25% volume fraction	eps_dp25	0.7	10
Real permeability of nanoparticles at 25% volume fraction	mu_p25	1.5	10
Imaginary permeability of nanoparticles at 25% volume fraction	mu_dp25	0.7	10
Permittivity of free space	eps_o	8.85E-12 F/m	SOURCE?
Time for diffusion	t_diff	10 hrs = 36000s	NA
Time for powered heating	t_heat	300	NA
Cooling time after t_heat followed by model	t_cool	300	NA
Volume of individual particles	V_particles	6.545*10^{-23} m^3	NA
Lethal CEM43°C for tumor	t43_tum	600 s	2
Lethal CEM43°C for liver tissue	t43_tiss	20400 s	3

VIII. Appendix B: Mesh Convergence

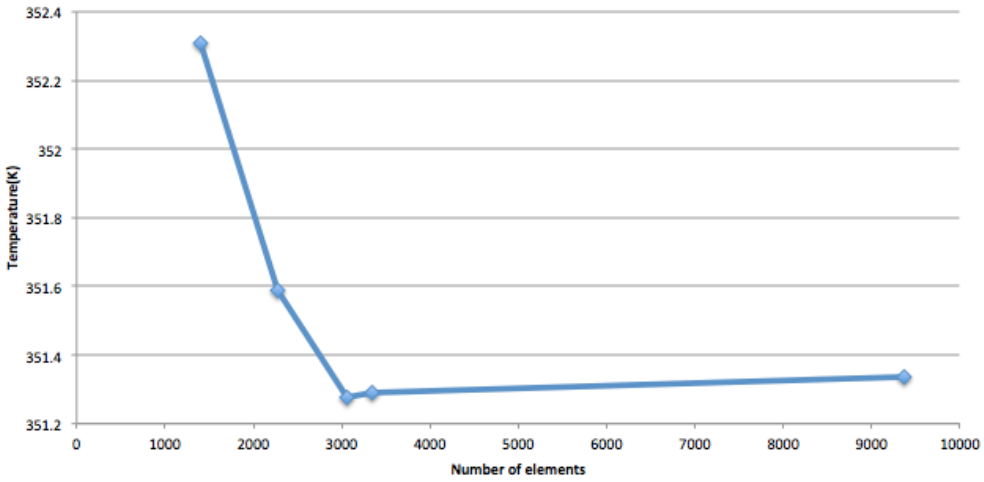

FIGURE 15. Mesh convergence analysis.

Figure 15 shows a mesh convergence analysis at a point at the interface between tissue and probe. We can see that with increasing refinement, i.e. the inclusion of more elements, the temperature profile converges on the plateaued region seen after 3000 elements are used. This indicates that using mesh densities higher than approximately 3000 triangular elements is appropriate for eliminating discretization error caused by meshing.

IX. Appendix D: References

[1]American Cancer Society. (2013). *Cancer Facts & Figures 2013.*

[2]Bernstein, M., & Berger, M. (2008). *Neuro-oncology: The Essentials.* New York: Thieme.

[3]Chang, I. (2010). Considerations for Thermally Injury Analysis for RF Ablation Devices. *The Open Biomedical Engineering Journal, 4*(1), 3-12.

[4]Hilger, I., Hergt, R., Hiergeist, R., Schubert, H., & WA, K. (2001). Electromagnetic heating of breast tumors in interventional radiology: in vitro and in vivo studies in human cadavers and mice. *Radiology, 218*(2), 570-575.

[5]Jemal, A., Bray, F., Center, M., Ferlay, J., Ward, E., & Forman, D. (2011). Global cancer statistics. *CA: A Cancer Journal for Clinicians, 61*(2), 69-90.

[6]Kasevich, R., Dwyer, A., & Guerreri, B. (1986). *Patent No. 4612940.* United States of America.

[7]Kim, B., Han, G., Toley, B., Kim, C.-k., Rotello, V., & Forbes, N. (2010). Tuning Payload Delivery in Tumour Cylindroids using Gold Nanoparticles. *National Nanotechnology, 5*(6), 465-472.

[8]Lubner, M., Brace, C., Hinshaw, J., & Lee, F. (2010). Microwave Tumor Ablation: Mechanism of Action, Clinical Results, and Devices. *Journal of Vascular and Interventional Radiology, 21*(8), 192-203.

[9]Milenic, D., E, B., & M, B. (2004). Antibody-targeted radiation cancer therapy. *Nature Reviews Drug Discovery, 3*(6), 488-498.

[10]Pearce, J., Cook, J., & Emelianov, S. (2010). Ferrimagnetic Nanoparticles Enhance Microwave Heating for Tumor Hyperthermia Therapy. *Annual International Conference of the IEEE EMBS*, (pp. 2751-2754). Buenos Aires.

[11]Sakran, F., Copty, A., Golosovsky, M., Davidov, D., & Monod, P. (2004). Scanning Ferromagnetic Resonance Microscopy and Resonant Heating of Magnetite Nanoparticles: Demonstration of Thermally Detected Magnetic Resonance. *Applied Physics Letters, 84*(22), 4499.

[12]Salloum, M., Ma, R., & Zhu, L. (2008). An in-vivo experimental study of temperature elevations in animal tissue during magnetic nanoparticle hyperthermia. *International Journal of Hyperthermia, 24*(7), 589-601.

[13]Wongtrairat, W., Phasukkit, P., Tungjitkusolmun, S., & Nantivatana, P. (2011). The Effect of Slot Sizes on Non-Asymmetry Slot Antenna for Microwave Coagulation Therapy. *International Journal of Bioscience, Biochemistry and Bioinformatics, 1*(3), 192-198.

[14]World Health Organization: International Agency for Research on Cancer. (2008). *World Cancer Report 2008.* Lyon.